# High-resolution scanning thermal probe with servocontrolled interface circuit for microcalorimetry and other applications

J.-H. Lee
*ECE Department, University of Wisconsin, Madison, Wisconsin 53706*

Y. B. Gianchandani[a)]
*ECE Department, University of Wisconsin, Madison, Wisconsin 53706*
*and EECS Department, University of Michigan, Ann Arbor, Michigan 48109*

(Received 30 November 2003; accepted 5 January 2004; published 22 April 2004)

This article presents a scanning thermal microscopy sensing system equipped with a customized micromachined thermal imaging probe and closed loop interface circuit. The micromachined thermal probe has a thin film metal bolometer sandwiched between two layers of polyimide for high thermal isolation and mechanical flexibility, and a tip with a diameter of approximately 50 nm which provides fine spatial resolution. The circuit includes a proportional-integral (PI) controller which couples to a Wheatstone bridge circuit in which the bolometer forms one leg. The PI controller adjusts power supplied to thermal probe, compensating change in heat loss from probe tip to sample and keeping the resistance bridge balanced. It permits precise control of probe temperature to within 2.3 mK, and widens its applications to microcalorimetry. The probe is used in thermal mapping and microcalorimetry applications. A calibration method based on microcalorimetric measurements of melting temperature is presented for the probe. Scanning thermal images show a high signal-to-noise ratio of 15.7 for 300 nm thick photoresist in which the minimum detectable thermal conductance change is $<23$ pW/K (which corresponds to a topographic change of 7.2 nm). Subsurface scans show a signal-to-noise ratio of 15.5 for variation of 1.0% in thermal resistance for a topographically smooth surface. © *2004 American Institute of Physics.*
[DOI: 10.1063/1.1711153]

## I. INTRODUCTION

In the past decade, scanning thermal microscopy (SThM) has drawn increasing interest for a variety of diagnostic applications, ranging from microcalorimetry to ultralarge scale integration (ULSI) lithography research to cellular diagnostics in biochemistry. An early example was the use of a thermal probe to map the latent image of exposed but undeveloped photoresist to measure photoacid generation and diffusion independently from the developing step.[1,2] Thermal probes have also been used for data storage and other applications.[3–6] Since they offer subsurface mapping capability, thermal probes also facilitate studies of intracellular features in bio-related research. To best meet the needs of many of these applications, which require the scanning of soft materials, thermal probes should have very low mechanical spring constants. In other cases, they must offer very high thermal isolation to minimize the thermal load presented to the sample. Both of these needs can be met by the use of a polymer for the probe shank.

Since SThM was introduced in 1986 by Williams and Wickramasinghe, probes using various thermal sensors have been developed. These include the thermocouple,[7–11] the bolometer or wire resistor,[12,13] Schottky diode,[14,15] and bimaterial cantilever.[16,17] In a resistive bolometer probe, the device is used both as a heater and as a sensor, making it suitable for applications such as thermal conductance mapping and microcalorimetry. Both temperature and thermal conductance of the sample can be detected from the fractional change in probe resistance. Wollaston wire probes are commercially available[18] and have been used for various thermal analyses.[13,19–21] This device uses a platinum/rhodium (90/10) thermal resistor. The probe is made of a wire with a thin core of 5 $\mu$m diameter surrounded by a thick silver cladding of 75 $\mu$m diameter. The exposed filament with a length of approximately 200 $\mu$m is the thermal element. In contrast, the probe used in this effort is a lithographically micromachined device that has been developed in a previous effort by our group. A thin-film metal bolometer is sandwiched between two layers of polyimide, forming a cantilever 300–400 $\mu$m in length and 50–150 $\mu$m wide.[1,22]

A Wheatstone bridge, which is commonly used for a variety of sensors such as piezoresistive pressure sensors, strain gauges, and thermistors, is also suitable for the readout of a bolometer probe. It can not only be integrated with the device but also allows a differential measurement that offers a higher common-mode noise rejection than a single-element measurement. However, the rest of the interface circuit, which has a major impact on the overall performance, must be carefully tailored for the probe. Historically, methods of converting the bridge resistance variation into currents or voltages for measurement have been plagued by problems of nonlinearity and restricted dynamic range.[23] To overcome the drawbacks of resistance-to-voltage conversion, many efforts have been made to convert resistance variation to

[a)]Electronic mail: yogesh@umich.edu

 

frequency,[24–26] to duty cycle/time,[27,28] and to both of them.[29] These approaches are constrained by switching delays causing nonlinearity between frequency (or pulse width) and resistance change, are expensive to implement, and are not adequate to operate a microbolometer in constant temperature mode with low noise.

This article presents a scanning thermal microscopy sensing system consisting of ultracompliant micromachined thermal probe and a closed loop analog interface circuit with a temperature-controllable proportional integral (PI) controller.[30,31] The interface circuit provides operation in constant temperature mode at user-specified temperatures. This is an important feature for microcalorimetry applications that require measurement of melting point and glass transition temperature of polymer films. It is tailored to the characteristics of the polyimide probe with regard to achieving temperature controllability and a fast thermal response. Various applications such as surface and subsurface thermal conductance mapping and melting temperature measurements are used to demonstrate the capabilities of the overall system.

## II. SENSOR ELEMENT

### A. Fabrication

Polyimide shank scanning thermal probes which use both, a bolometer,[22] and a thermocouple,[32] as the transducing element have been reported. In both cases the transducing element is made from thin metal films embedded between two layers of polyimide, allowing the probe to be mechanically ultracompliant. At one end of the cantilever the metal thin film protrudes through an opening in the lower polyimide layer, where it is molded into a pyramidal tip by a notch that is anisotropically wet-etched into the substrate. The fabrication process provides a tip diameter of about 50 nm by sharpening the notch using nonuniform oxide growth. The tip and a portion of the probe shank are then released from the substrate by etching an underlying sacrificial layer. As shown in Fig. 1, the released length is then folded over to extend past the die edge for clearance and held in place by a thermocompression bond across a thin film of Au which is deposited as the final layer on top of the polyimide. This layer also serves as a mirror to permit simultaneous operation of the probe as an atomic force microscope probe. The whole fabrication process is performed below 350 °C, and is compatible with post-complementary metal-oxide semiconductor fabrication, permitting the potential integration of an interface circuit. Typical dimensions of the probes after assembly are 360 $\mu$m length, 120 $\mu$m width, and 3.5 $\mu$m thickness with Cr/Ni (200/1000) for the tip and Cr/Au (200/2000) for the lead, which provides bolometer resistance about 45 $\Omega$. This results in bolometer type probes that offer measured spatial resolution of $<50$ nm, and mechanical spring constant ranging from 0.1 to 0.3 N/m depending on the dimension of the probes.

### B. Operation

For limited temperature excursions in metal and semiconductor materials, the electrical resistance can be approximated as being linearly proportional to the average probe temperature $T_p$:

$$R_p = R_o \times [1 + \mathrm{TCR} \times (T_p - T_0)], \tag{1}$$

where $R_o$ is the resistance at temperature $T_o$ and TCR is the temperature coefficient of resistance. Thermal probe resistance is composed of resistance of the tip, which serves as a sensing element as well as a heater, and parasitic resistance along the shank, as shown in Fig. 2. The sensing element is made of a thin film of Ni–Au, where along the shank a relatively thick Au layer that overlaps the Ni trace provides

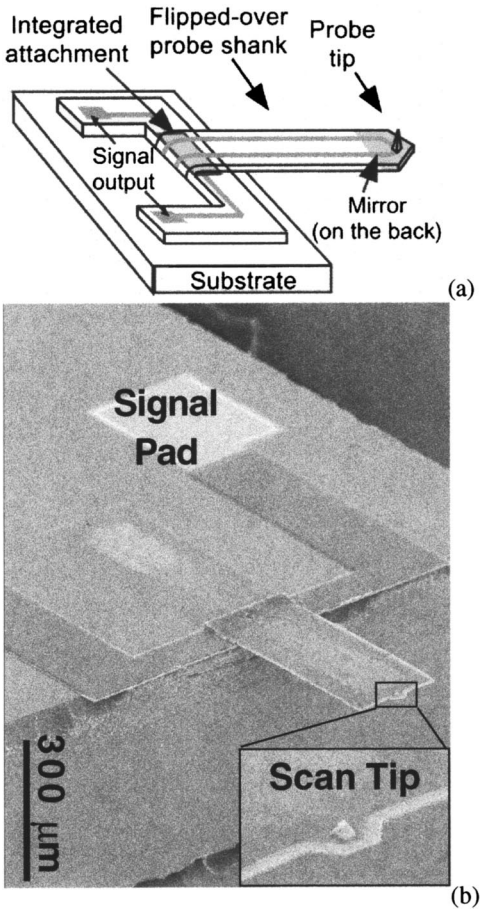


FIG. 1. Ultracompliant scanning thermal probe (a) schematic of a polyimide thermal probe (b) scanning electron microscopy image of a fabricated thermal probe with a close up of the scan tip.

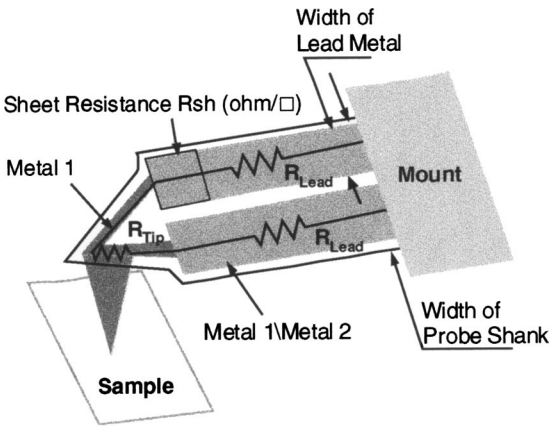


FIG. 2. Schematic of micromachined bolometer.

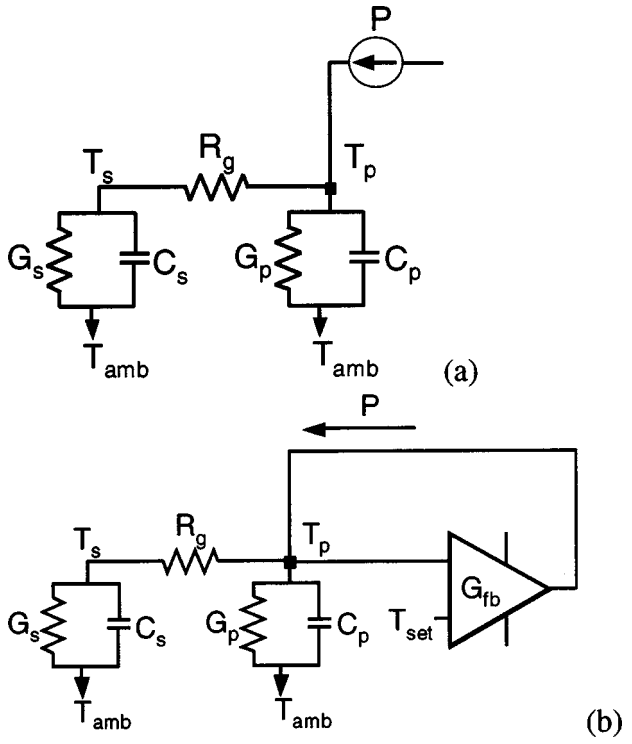


FIG. 3. Equivalent diagram for thermal sensing system operating (a) in a constant power mode and (b) in a constant-temperature mode. $G_s$ and $C_s$ are thermal conductance and capacitance of the sample, respectively. $R_g$ is thermal resistance of gap between probe tip and sample surface. $T_s$ and $T_p$ are the average temperature of sample surface and probe, respectively. $T_{\text{amb}}$ is the ambient temperature.

high electrical conductance. The increased thermal conductance along the shank permits localized heating around the tip area, helping to increase sensitivity.

If the parasitic resistance can be ignored, the resistance change is linearly proportional to the square of the applied current over a wide range including the operating conditions. Therefore, Eq. (1) can be rewritten as

$$R_p = R_o \times [1 + \text{TCR} \times \beta \times I_p^2], \tag{2}$$

where $\beta$ is a unit-converting constant in $\text{K/A}^2$, and $I_p$ is the current through the probe. According to Eq. (2), the probe resistance is linearly proportional to the applied power. (This has been experimentally verified. A typical value for the $\text{TCR} \times \beta$ factor is 520.8 when the current is in amperes.)

The thermal probe can operate either in a constant power mode or in a constant temperature mode. As shown in Fig. 3(a), $T_p$ is linearly proportional to change in thermal conductance ($G_s$) of a sample during scanning if change in heat loss through thermal conductance of the probe shank ($G_p$) is negligible and scanning speed is very low. Therefore, the probe resistance can be used to map the thermal conductance of the surface. In constant temperature mode, the probe current compensates for heat lost through probe tip, Fig. 3(b). The compensating power can be used to map the thermal conductance changes in the sample. The operating temperature can be easily controlled electrically. The thermal response time of the probe is significantly reduced as the external interface

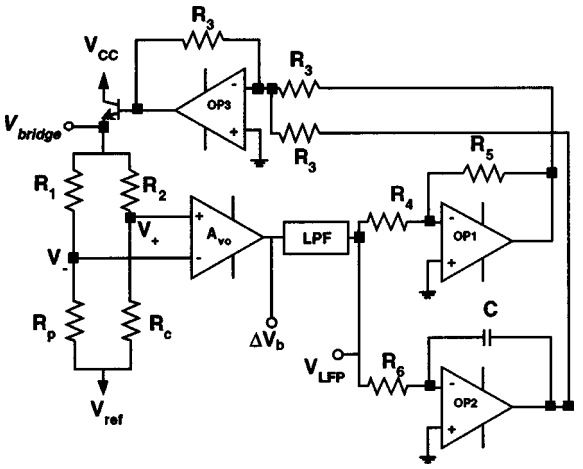


FIG. 4. Servocontrolled interface circuit for constant temperature mode operation.

circuit provides instantaneous power to keep the probe at a constant temperature so that effective thermal conductance increases.

## III. INTERFACE CIRCUIT

The feedback-controlled interface circuit is depicted in Fig. 4. The resistor bridge circuit is composed of four resistors, $R_1$, $R_2$, $R_c$, and $R_p$. Resistor $R_c$ is the temperature control resistor and used to set the operating temperature of $R_p$. When the bridge resistors are balanced, the voltage $\Delta V_b$ becomes zero and satisfies

$$\frac{R_1}{R_p} = \frac{R_2}{R_c}. \tag{3}$$

If Eq. (3) is not valid, an error voltage $V^+ - V^-$ is amplified by an instrumentation amplifier and then fed into a proportional-integral (PI) controller, which provides compensation current $I_p$ to keep the bridge balanced. Since the average probe temperature increases or decreases with the compensation power, the probe resistance $R_p$ is adjusted by $I_p$ through the PI controller until the relationship of Eq. (3) is satisfied.

The PI controller is realized by using an integrator, an inverting amplifier, a summing amplifier, and a current buffer. The proportional gain $K_p$ and the integral gain $K_i$ are determined by $R_5/R_4$ and $1/R_6C$. Since the range of $R_6$ is limited on the low side by the output current of the preceding operational amplifier, the capacitance of the integrator is chosen to be 10 nF in order to acquire high integral gain $K_i$ of $10^4$. A low pass filter can be located between the voltage differential amplifier and the PI controller. It plays the role of removing noise which is at frequencies larger than signal bandwidth.

## IV. MEASUREMENT

### A. Circuit performance

The performance of the bridge feedback circuit is confirmed by changing $R_c$ to mimic operating temperature change as presented in Fig. 5. The voltage at the top of the

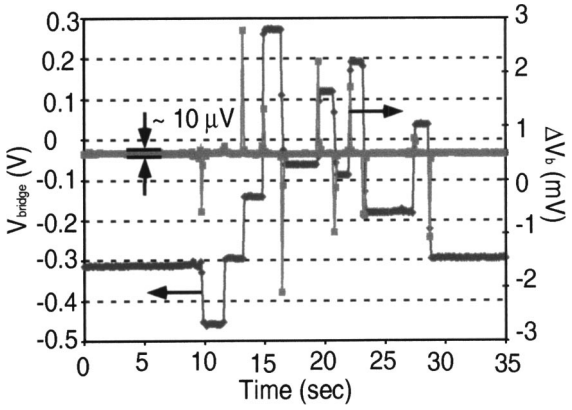


FIG. 5. Measurement of temperature controllability of closed loop interface circuit: $V_{\text{bridge}}$ is the supply voltage to the bridge, as shown in Fig. 4, whereas $\Delta V_b$ is proportional to the differential output of the bridge. As $R_c$, the temperature control resistor is stepped through various values, the supply voltage to the bridge changes, restoring the differential output to its neutral value. This demonstrates the operation of the servo-control circuit.

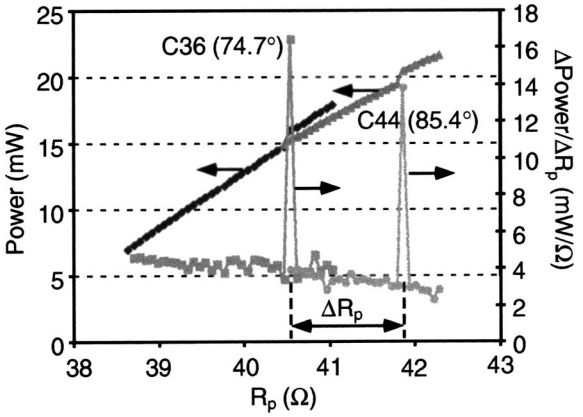


FIG. 6. Melting point measurement and temperature calibration using closed loop interface circuit for materials with known melting temperatures ($C_{36}H_{74}$ and $C_{44}H_{90}$). Abrupt changes in the slope of the power to resistance (i.e., power to tip temperature) indicate a phase transition in the sample. This can be used to calibrate the bolometer at the probe tip.

bridge circuit $V_{\text{bridge}}$ and the voltage difference between the two intermediate bridge nodes $\Delta V_b$ are observed for the ability of the circuit to track these changes. The temperature control resistor $R_c$ is stepped through various values to vary the probe temperature. Figure 5 shows that $V_{\text{bridge}}$ changes to compensate for the change in the bolometer temperature caused by the change in $R_c$. It is observed that the variation in $\Delta V_b$ is kept less than 10 $\mu$V in steady state, which means the minimum controllable probe resistance is 0.56 m$\Omega$ and the minimum controllable probe temperature is 2.3 mK according to Eqs. (4), (5), and (6):

$$\left|\frac{R_{\text{po}}+\Delta R_p}{R_{\text{po}}+R_1}-\frac{R_c}{R_c+R_2}\right|\cong\frac{\Delta V_b}{V_{\text{bridge}}-V_{\text{ref}}}, \tag{4}$$

$$\Delta R_p\cong\frac{10\times10^{-6}}{5.0}\times(R_{\text{po}}+R_1)=0.56\ (\text{m}\Omega), \tag{5}$$

$$\Delta T_p\cong\frac{5.6\times10^{-4}}{R_{\text{po}}\times\text{TCR}}=2.3\ (\text{mK}), \tag{6}$$

where $R_{\text{po}}$ is 30 $\Omega$, $R_1$ is 250 $\Omega$, and TCR is 8000 ppm/K.

### B. Temperature calibration

Tip temperature of a bolometer probe in constant temperature mode is calibrated using two hydrocarbons whose melting temperatures are already known. The average temperature of the probe can be calculated from the probe resistance, and the average temperature is converted into the actual tip temperature, which is equal to or very close to the melting point of the sample hydrocarbons.

Figure 6 shows the melting point measurement of two hydrocarbons, hexatriacontane ($C_{36}H_{74}$) and tetratetracontane ($C_{44}H_{90}$), whose melting point temperatures are well-controlled and characterized. The probe resistance $R_p$ is increased by ratcheting up the temperature control resistance $R_c$ in the bridge circuit of Fig. 4 and the compensation power is measured versus $R_p$. The power can be obtained from

$$P_c=\left(\frac{V_{\text{bridge}}-V_{\text{ref}}}{R_1+R_p}\right)^2\times R_p. \tag{7}$$

There is a transition value of $R_p$ for each hydrocarbon where $\Delta P_c/\Delta R_p$ changes abruptly. The $\Delta R_p$ in Fig. 6 corresponds to the change in the average probe temperature. The calibration factor $k$ can be defined from the measurement as

$$k\equiv\frac{T_p-T_o}{T_{\text{tip}}-T_o}\quad(0<k<1), \tag{8}$$

where $T_p$ is the average temperature of the probe corresponding to $R_p$, $T_o$ is the room temperature, and $T_{\text{tip}}$ is the tip temperature of the probe which is equal to the melting temperature. If the TCR of the probe metal is known, the calibration factor $k$ can be calculated as shown below

$$k\cong\frac{\Delta R_p}{R_o\times\text{TCR}\times(T_{M1}-T_{M2})}\quad(0<k<1), \tag{9}$$

where $T_{M1}$ and $T_{M2}$ are the melting temperatures of the known materials, in this case, $C_{36}H_{74}$ and $C_{44}H_{90}$. According to Fig. 6, since $R_o$ is 37.5 ($\Omega$), $T_{M1}-T_{M2}$ is 10.7 (K), $\Delta R_p$ is 1.32 ($\Omega$), and TCR is 7925 ($\mu\Omega$/K) for a probe, $k$ becomes 0.41. As $k$ increases, so does the average temperature of probe shank. The value of $k$ depends not only on the geometry of the probe, but also on the sample and its substrate, and on the ambient conditions. It tends to mostly lie between 0.25 and 0.5.

### C. Surface scan

Topographic and thermal images of developed 350 nm thick Shipley UV6 photoresist are shown in Fig. 7. The thermal image was obtained by scanning at 45 °C tip temperature using the dc closed-loop interface circuit of Fig. 4. The change in the compensation power delivered to the thermal probe is directly used to estimate the change of the thermal conductance of a sample. When the film is thin compared to the probe diameter, the heat transfer between the probe tip

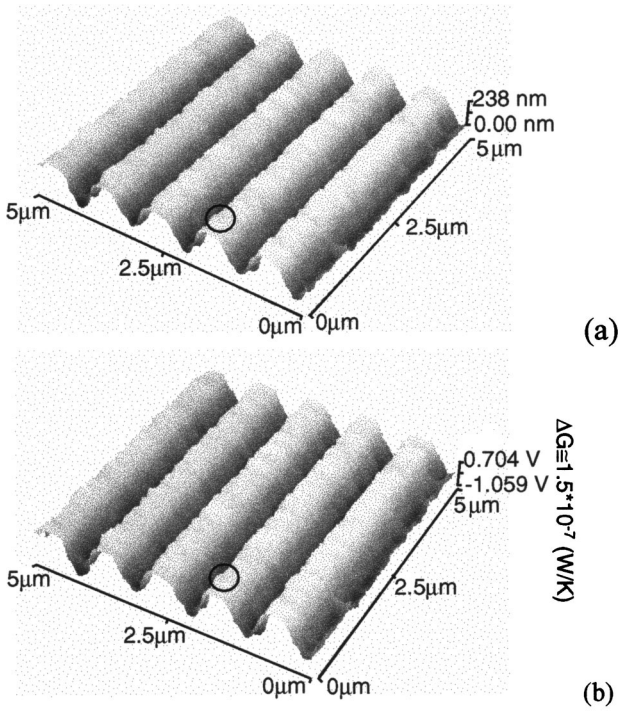


FIG. 7. Scan results of developed 238 nm thick UV6 photoresist scanned at 45 °C tip temperature using dc closed-loop interface circuit (a) topographic scanning image and (b) thermal scanning image.

and silicon substrate can be modeled as that through a cylinder. The heat loss ($P_s$) to the silicon substrate through the tip can be expressed as

$$P_s = (T_{\text{tip}} - T_0) \times A_0 \times k_s / H, \tag{10}$$

where $T_{\text{tip}}$ is the probe tip temperature, $A_0$ is the tip-sample contact area, $k_s$ is the thermal conductivity of photoresist, and $H$ is the photoresist thickness. This formula assumes that the substrate of the sample, i.e., the material below the thin film, remains at room temperature. Since the compensation power $P_c$ delivered to the thermal probe and sample to keep the probe average temperature at $T_p$ is given by Eq. (7), the change in thermal conductance of sample during a scan can be represented as

$$\Delta G = \frac{P_{c1} - P_{c2}}{T_{\text{tip}} - T_o} = \left[ \left( \frac{V_{\text{bridge1}} - V_{\text{ref}}}{R_1 + R_p} \right)^2 - \left( \frac{V_{\text{bridge2}} - V_{\text{ref}}}{R_1 + R_p} \right)^2 \right] \times \frac{R_p}{T_{\text{tip}} - T_o} \quad \text{(W/K)}. \tag{11}$$

This formula can be used to calculate the variation of thermal conductance across a sample by measuring the variation in power dissipated for a constant temperature map. Even though $P_s$ is not equal to $P_c$, $\Delta P_s$ is regarded as equal or very close to $\Delta P_c$ because the wasted heat loss through probe shank can be considered constant in constant temperature operation. Thus, mapping the power in constant temperature mode provides an accurate representation of the change in thermal conductance of the sample.

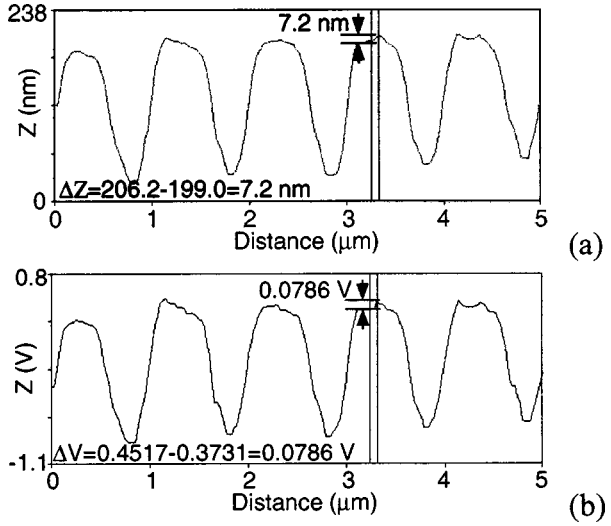


FIG. 8. Scan results of developed 238 nm thick UV6 photoresist scanned at 45 °C tip temperature using dc closed-loop interface circuit (a) topographic line scan across photoresist patterns and (b) thermal line scan across photoresist patterns.

The full scale thermal conductance change can be calculated from Eq. (11). For the thermal image of Fig. 7(b), $R_1$ and $R_p$ are 250 and 25 Ω. The reference voltage $V_{\text{ref}}$ is $-4.0$ V and $T_p$ is 318 K. The voltage at the top of the bridge $V_{\text{bridge}}$ is equal to the output voltage divided by the voltage gain of 100. The calculated variation in thermal conductance from Si substrate to the photoresist film is $1.5 \times 10^{-7}$ W/K. It may overestimate the actual thermal conductance change because the variation in the wasted power through the probe shank due to the slight change in the gap between the probe shank and sample surface was ignored in Eq. (11). The topographic and thermal images look very similar because the

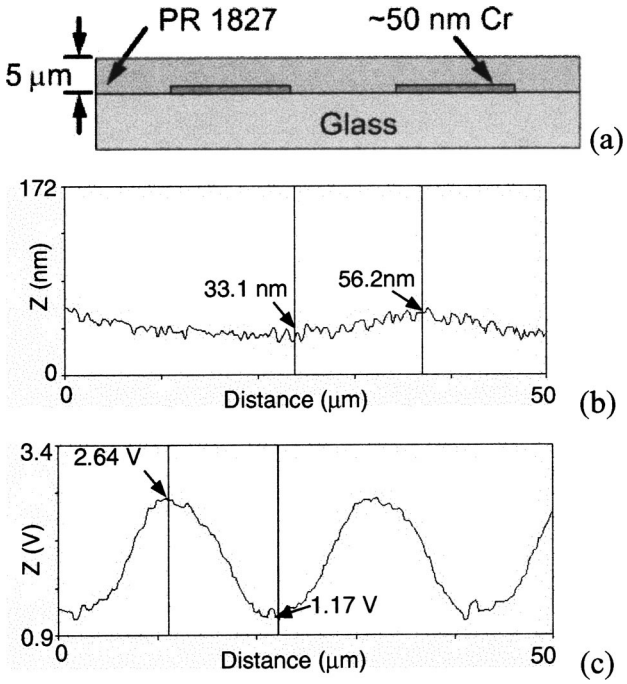


FIG. 9. Subsurface scan results (a) cross-sectional view of sample, (b) topographic line scan, and (c) thermal line scan for 50 nm thick Cr patterns with 5 μm thick photoresist coated on it using the dc closed loop interface circuit.

TABLE I. Measured specifications of closed loop thermal sensing system.

| Specifications | Measured values |
|---|---|
| Tip diameter | 50 nm |
| Lateral spatial resolution | $<50$ nm[a] |
| Topographical resolution | 1 nm[a] |
| SNR (238 nm thick UV6) | 15.7 |
| $\Delta R$ resolution | $<0.56$ m$\Omega$ (controllable) |
| Tip temperature resolution | $<2.5$ mK (controllable) |
| Detectable Th. conductance change | $<23$ (pW/K) |

[a]Reference 1.

thermal conductance image contains both the topographic and the thermal conductivity information, and the topographic change is the only factor in this sample. Figure 8 shows the variations in topographic and thermal signal across photoresist line patterns. The signal-to-noise ratio is 15.7 for thermal measurement. The resolvable thermal conductance change was calculated to be $2.3\times10^{-11}$ W/K for a thickness change of 7.2 nm based on Eq. (1).

In contrast to the micromachined polyimide probe, for a Wollaston wire probe the nominal resistance and spring constant are 2.1 ohm and 5 N/m, respectively. Since the diameter of this probe is 100 times bigger than that of the micromachined probe, the change in its minimum detectable thermal conductance is about $10^4$ times 23 pW/K because the detectable thermal conductance change is linearly proportional to tip area when the detectable limit of topographic change is the same as 7.2 nm.

It is also evident from Fig. 8 that the thermal scan is able to detect features which are $<50$ nm in spatial extent in the topographic scan. This is consistent with the sub-50 nm lateral spatial resolution reported with an open-loop interface circuit by Li and Gianchandani.[1]

### D. Subsurface scan

Scanning thermal microscopy offers an effective tool for mapping subsurface variations in samples. In order to test this feature, a test sample was prepared in which 50 nm-thick Cr was patterned on a glass substrate and then coated with 5 $\mu$m-thick Shipley 1827 photoresist to planarize the sample. Photoresist is a very good thermal insulator (e.g., polymethyl methacrylate has a thermal resistivity of 0.193 W/m/K). This sample effectively provided a surface in which there was no pattern-related topographic change, and the variation in thermal conductance caused by the Cr pattern was substantially insulated from the surface. It is estimated that this variation amounted to a 1.0% change in a thermal resistance of $1.0\times10^{10}$ (K/W). The scan resuts are shown in Fig. 9: The schematic in Fig. 9(a) illustrates the sample; the topographic scan in Fig. 9(b) shows that there is 23 nm variation across the sample surface, but it does not correspond to the pattern; Fig. 9(c) shows that there is a very clear and significant variation in the thermal signal which corresponds to the Cr pattern. According to this scan, the signal-to-noise ratio is in excess of 15.

The overall performance of the probe is summarized in Table I.

## ACKNOWLEDGMENTS

This work was funded in part by the Semiconductor Research Corporation Contract No. 98-LP-452.005. The Center for NanoTechnology, University of Wisconsin-Madison, is supported in part by DARPA/ONR Grant Nos. MDA 972-00-1-0018, and MDA 972-99-1-0013. Valuable discussions with Dr. M.-H. Li and Dr. R. Tate are gratefully acknowledged. The authors are also grateful to Professor F. Cerrina for supplying the UV6 photoresist samples, and to both him and Dr. Leonidas Ocola for identifying the need for this research and encouraging it.

[1] M.-H. Li and Y. B. Gianchandani, Sens. Actuators, A **104**, 236 (2003).
[2] L. E. Ocola, D. Fryer, P. Nealey, J. dePablo, F. Cerrina, and S. Kämmer, J. Vac. Sci. Technol. B **14**, 3974 (1996).
[3] H. K. Wickramasinghe, Sci. Am. **Oct.**, 98 (1989).
[4] P. Vettiger, M. Despont, U. Drechsler, U. Dörig, W. Häberle, M. I. Lutwyche, H. E. Rothuizen, R. Stutz, R. Widmer, and G. K. Binnig, IBM J. Res. Dev. **44**, 323 (2000).
[5] A. Majumdar, Annu. Rev. Mater. Sci. **29**, 505 (1999).
[6] A. Hammiche, D. J. Hourston, H. M. Pollock, M. Reading, and M. Song, J. Vac. Sci. Technol. B **14**, 1486 (1996).
[7] A. Majumdar, J. Lai, M. Chandrachood, O. Nakabeppu, Y. Wu, and Z. Shi, Rev. Sci. Instrum. **66**, 3584 (1995).
[8] Y. Suzuki, Jpn. J. Appl. Phys., Part 2 **35**, L352 (1996).
[9] Y. B. Gianchandani and K. Najafi, IEEE Trans. Electron Devices **44**, 1857 (1997).
[10] G. Mills, H. Zhou, A. Midha, L. Donaldson, and J. M. R. Weaver, Appl. Phys. Lett. **72**, 2900 (1998).
[11] H. Zhou, A. Midha, G. Mills, S. Thoms, S. K. Murad, and J. M. R. Weaver, J. Vac. Sci. Technol. B **16**, 54 (1998).
[12] R. B. Dinwiddie, R. J. Pylkki, and P. E. West, Therm. Conduct. **22**, 668 (1994).
[13] A. Hammiche, H. M. Pollock, M. Song, and D. J. Hourston, Meas. Sci. Technol. **7**, 142 (1996).
[14] R. C. Davis, C. C. Williams, and P. Neuzil, Appl. Phys. Lett. **66**, 2309 (1995).
[15] T. Leinhos, M. Stopka, and E. Oesterschulze, Appl. Phys. A: Mater. Sci. Process. **66**, S65-9 (1998).
[16] J. R. Barnes, R. J. Stephenson, C. N. Woodburn, S. J. O'Shea, M. E. Welland, T. Rayment, J. K. Gmzewski, and Ch. Gerber, Rev. Sci. Instrum. **65**, 3793 (1994).
[17] O. Nakabeppu, M. Chandrachood, Y. Wu, J. Lai, and A. Majumdar, Appl. Phys. Lett. **66**, 694 (1995).
[18] Veeco, www.veeco.com
[19] G. B. M. Fiege, A. Altes, R. Heiderhoff, and L. J. Balk, J. Phys. D **32**, L13 (1999).
[20] D. Fryer, P. Nealey, and J. de Pablo, Macromolecules **33**, 6439 (2000).
[21] D. Fryer, P. Nealey, and J. de Pablo, J. Vac. Sci. Technol. B **18**, 3376 (2000).
[22] M.-H. Li and Y. B. Gianchandani, J. Vac. Sci. Technol. B **18**, 3600 (2000).
[23] D. J. Yonce, P. P. Bey, Jr., and T. L. J. Fare, IEEE Trans. Circuits Syst., I: Fundam. Theory Appl. **47**, 273 (2000).
[24] K. Mochizuki and K. Watanabe, *Proceedings on Instrumentation and Measurement Technology Conference* (IMTC, Waltham, MA, 1995), p. 339.
[25] J. H. Huijsing, G. A. Van Rossum, and M. van der Lee, IEEE J. Solid-State Circuits **SC-22**, 343 (1987).
[26] B. Gilbert, IEEE J. Solid-State Circuits **SC-11**, 852 (1976).
[27] A. Cichocki and R. Unbehauen, Sens. Actuators, A **24**, 129 (1990).
[28] F. M. L. van der Goes, P. C. De Jong, G. C. M. Meijer, *Proceedings IEEE International Conference on Solid-State Sensors and Actuators* (Transducers, Yokohama, Japan, 1993), p. 331.
[29] V. Ferrari, C. Ghidini, D. Marioli, and A. Taroni, Meas. Sci. Technol. **8**, 827 (1997).
[30] J.-H. Lee, M.-H. Li, and Y. B. Gianchandani, *Proceedings International Workshop on Thermal Investigations of ICs and Systems* (THERMINIC, Madrid, Spain, 2002), p. 111.
[31] J.-H. Lee, Ph.D. Dissertation, University of Wisconsin, Madison, 2003.
[32] M.-H. Li, J. J. Wu, and Y. B. Gianchandani, J. Microelectromech. Syst. **10**, 3 (2001).